Proximal structured sparsity regularization for online reconstruction in high-resolution accelerated MRI

13 December 2019

Ph.D. Thesis defense presented by
Loubna El Gueddari

Supervisors

Dr Nicolas Boulant — CEA *NeuroSpin and University Paris-Saclay*
Dr Philippe Ciuciu — CEA *NeuroSpin and* INRIA *Parietal*

Reviewers

Pr Carola-Bibiane Schönlieb — *Cambridge University*
Pr Angshul Majumdar — IIT *Delhi*

Examiners

Dr Rachid Deriche — INRIA ATHENA
Dr Lotfi Chaari — INP *Toulouse*
Pr Jean-Christophe Pesquet — *Centrale-Supelec and University Paris-Saclay*

High resolution imaging: Increasing the SNR

Ultra-high magnetic field

- Signal-to-Noise Ratio (SNR) increases with the field strength: SNR $\propto B_0^{1.65}$[1]

B_0=3T

7T

11.7T

- Particularly suited for the T_2^*-weighted imaging contrast

[1] Pohmann, Speck, and Scheffler 2016, *Magnetic resonance in medicine.*

High resolution imaging: Increasing the SNR

Ultra-high magnetic field

- Signal-to-Noise Ratio (SNR) increases with the field strength: SNR $\propto B_0^{1.65}$
- Particularly suited for the T_2^*-weighted imaging contrast[1]

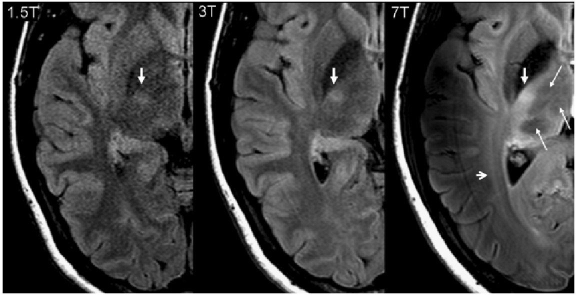

- 2017: 7 Tesla MR systems FDA-cleared & CE-marked for clinical practice

[1]Zwanenburg et al. 2010, *European radiology*.

High resolution imaging: Increasing the SNR
Multi-channel array coils

Parallel imaging: collect multiple k-space data using a multi-receiver coil to boost the SNR [2].

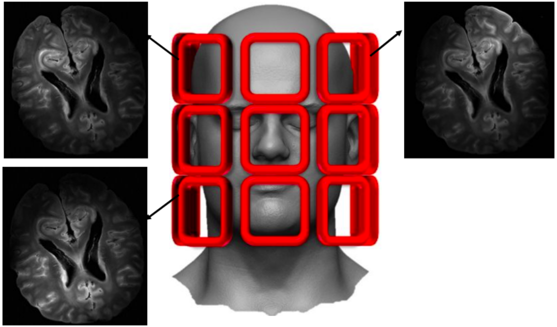

Illustration of multi-receiver coil (phased array).

[2] Roemer et al. 1990, *Magnetic Resonance in Medicine*

High resolution imaging: Increasing the SNR

Multi-channel array coils

Parallel imaging: collect multiple k-space data using a multi-receiver coil to boost the SNR [2].

Ex-vivo baboon brain acquired at 7T with a single channel and 32-channel receiver coils.

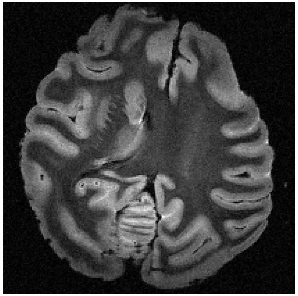

Single channel acquisition.

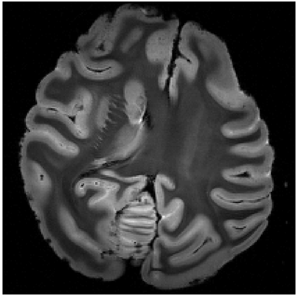

Multi-channel acquisition.

Courtesy Carole Lazarus

[2] Roemer et al. 1990, *Magnetic Resonance in Medicine*

Highest in vivo Human Brain data acquired at 7T

- Towards imaging at the meso-scale ($\simeq 100\mu m^2$ in plane)

- Highest in-vivo Human Brain MRI data collected at 7T[3]:
  - B_0 field strength: 7T
  - Multi-channel receiver coil: 32 Rx
  - Resolution: $0.12 \times 0.12 \times 0.6 mm^3$
  - Field of View: $20.28 \times 20.93 \times 1.26$ cm^3
  - Averages: 2
  - Total scan time: 50 min

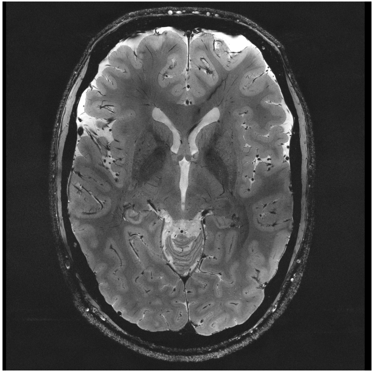

[3] Stucht et al. 2015, *PloS one*

Highest in vivo Human Brain data acquired at 7T

- Towards imaging at the meso-scale ($\simeq 100\mu m^2$ in plane)

- Highest in-vivo Human Brain MRI data collected at 7T [3]:
  - B_0 field strength: 7T
  - Multi-channel receiver coil: 32 Rx
  - Resolution: $0.12 \times 0.12 \times 0.6 mm^3$
  - Field of View: $20.28 \times 20.93 \times 1.26$ cm^3
  - Averages: 2
  - Total scan time: 50 min

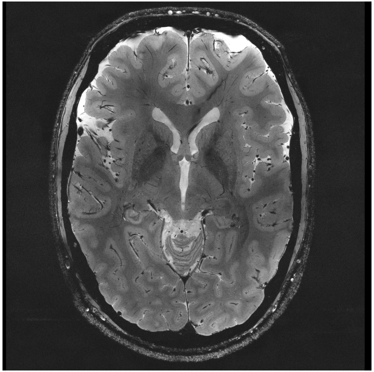

How can we speed-up the acquisition?

[3] Stucht et al. 2015, *PloS one*

Acquisition in MRI

Data collection in MRI is typically performed over a Cartesian grid:

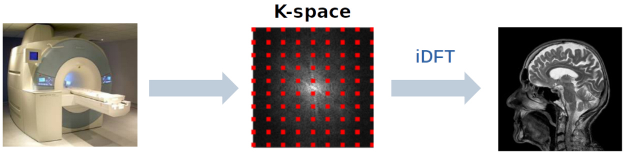

Nyquist-Shannon theory

$\uparrow$ resolution $\Rightarrow$ $\uparrow$ #samples

$\Downarrow$

Long acquisition times

> The sampling frequency should be at least twice the highest frequency contained in the signal

Harry Nyquist

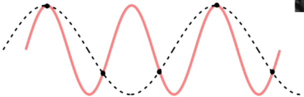

Acquisition in MRI

Data collection in MRI is typically performed over a Cartesian grid:

K-space

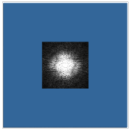

iDFT

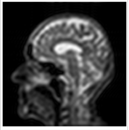

Nyquist-Shannon theory

↑ resolution ⇒ ↑ #samples

Long acquisition times

The sampling frequency should be at least twice the highest frequency contained in the signal

Harry Nyquist

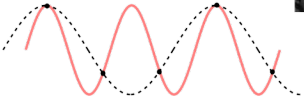

Acquisition in MRI

Data collection in MRI is typically performed over a Cartesian grid:

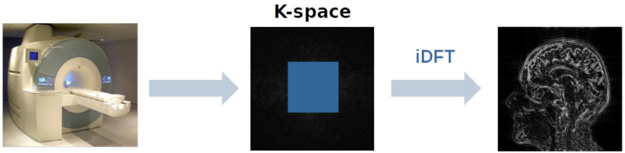

Nyquist-Shannon theory

$\uparrow$ resolution $\Rightarrow$ $\uparrow$ #samples

Long acquisition times

The sampling frequency should be at least twice the highest frequency contained in the signal

Harry Nyquist

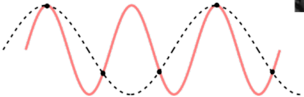

Acquisition in MRI

Data collection in MRI is typically performed over a Cartesian grid:

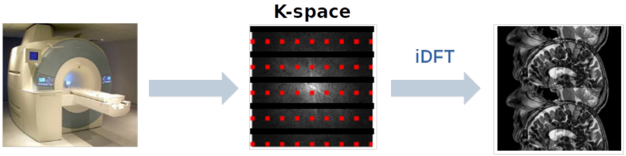

Nyquist-Shannon theory

$\uparrow$ resolution $\Rightarrow$ $\uparrow$ #samples

$\Downarrow$

Long acquisition times

The sampling frequency should be at least twice the highest frequency contained in the signal

Harry Nyquist

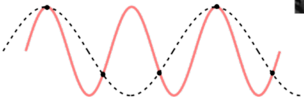

Compressed Sensing: Beyond Nyquist sampling rate

Sparsity

Compressed sensing[4,5] (CS) relies on three main assumptions:

1. Sparsity: Image to be reconstructed is represented by only a few non-zero coefficients in an transformed domain.

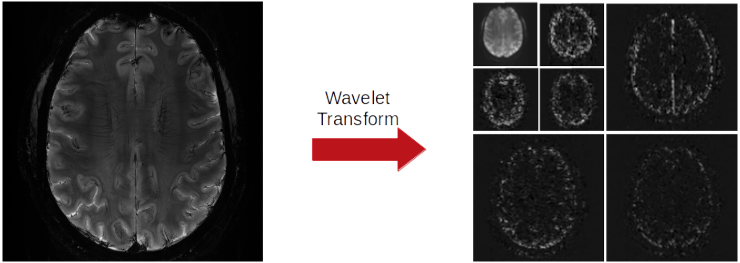

[4]Candès, Romberg, and Tao 2006, *IEEE Transactions on information theory*.
[5]Lustig, Donoho, and Pauly 2007, *Magnetic Resonance in Medicine*.

Compressed sensing[6,7] (CS) relies on three main assumptions:

1. Sparsity
2. Incoherence

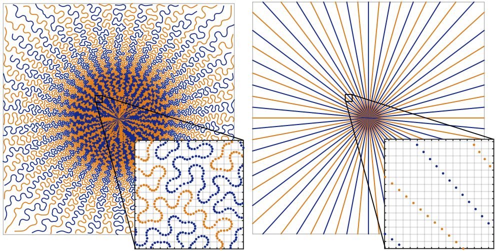

Sparkling VDS[8] Radial VDS

[6] Candès, Romberg, and Tao 2006, *IEEE Transactions on information theory*.
[7] Lustig, Donoho, and Pauly 2007, *Magnetic Resonance in Medicine*.
[8] Lazarus et al. 2019, *Magnetic Resonance in Medicine*

Compressed sensing[6,7] (CS) relies on three main assumptions:

1. Sparsity
2. Incoherence

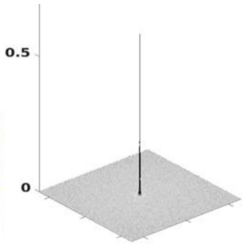

Sparkling VDS[8]

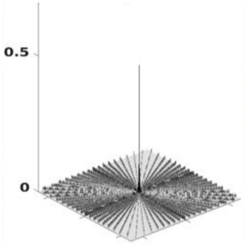

Radial VDS

[6] Candès, Romberg, and Tao 2006, *IEEE Transactions on information theory*.
[7] Lustig, Donoho, and Pauly 2007, *Magnetic Resonance in Medicine*.
[8] Lazarus et al. 2019, *Magnetic Resonance in Medicine*

Compressed Sensing: Beyond Nyquist sampling rate

Non-linear reconstruction: when sparsity meets incoherence

1. Sparsity
2. Incoherence
3. Sparsity-promoting reconstruction: $\hat{\boldsymbol{x}} = \underset{\boldsymbol{x} \in \mathbb{C}^N}{\arg\min} \frac{1}{2} \| \mathcal{F}_\Omega \boldsymbol{x} - \boldsymbol{y}_\Omega \|_F^2 + \lambda \| \boldsymbol{\Psi} \boldsymbol{x} \|_1,$

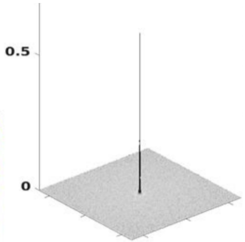

Sparkling VDS[9]

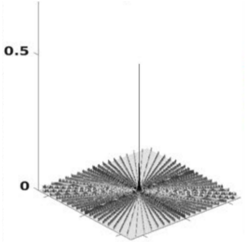

Radial VDS

[9] Lazarus et al. 2019, *Magnetic Resonance in Medicine*

Successful application of Compressed Sensing in MRI[10]

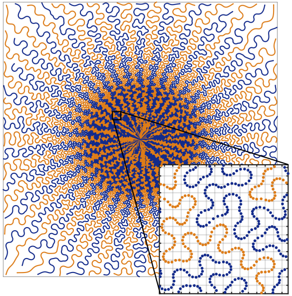

Sparkling VDS

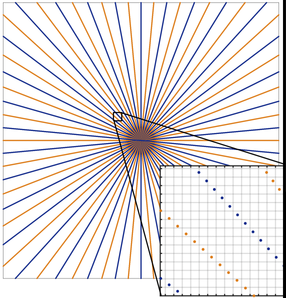

Radial VDS

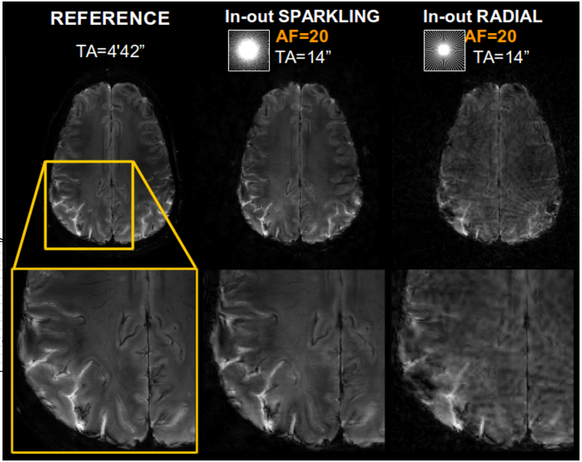

[9] Lazarus et al. 2019, *Magnetic Resonance in Medicine*

Compressed Sensing: Beyond Nyquist sampling rate

Successful application of Compressed Sensing in MRI[10]

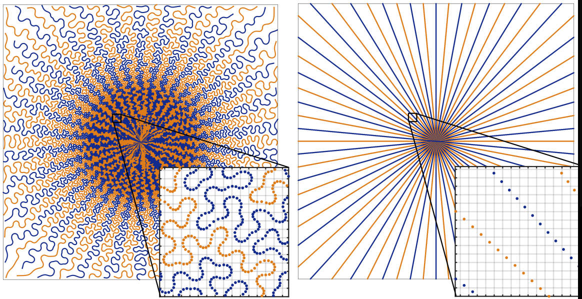

Sparkling VDS Radial VDS

- Reconstruction takes 15 min for a 2D slice!

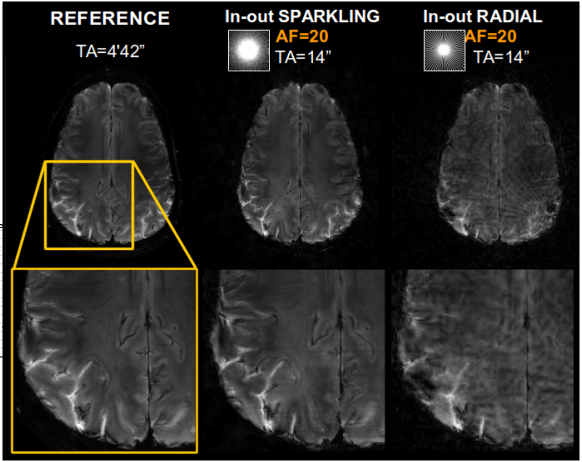

[9]Lazarus et al. 2019, *Magnetic Resonance in Medicine*

The reconstruction bottleneck for clinical practice

Having a feedback directly on the scanner:

- Improve the protocol planning

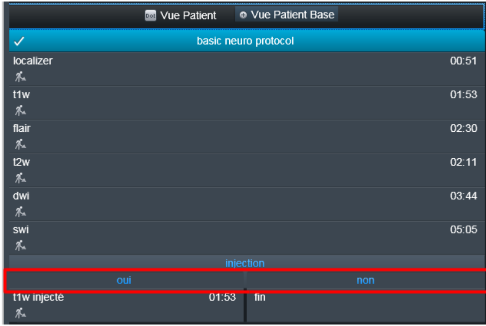

The reconstruction bottleneck for clinical practice

Might want to have a feedback directly on the scanner:

- Improve the protocol planning
- Sanity check:
  - Motion artifact
  - Artifacts caused by other devices

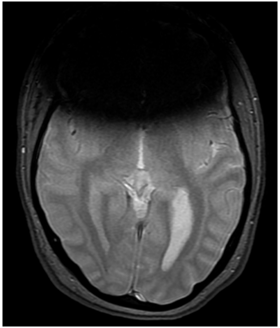

Figure: Orthodontic braces causing loss of signal in GRE/T_2^*-w images[11]

[11] Krupa and Bekiesińska-Figatowska 2015, *Polish journal of radiology*

The reconstruction bottleneck for clinical practice

Might want to have a feedback directly on the scanner:

- Improve the protocol planning
- Sanity check:
  - Motion artifact
  - Artifacts caused by other devices

Provide a fast and reliable
feedback to take a decision on the protocol.

Toward fast high-resolution imaging in clinical practice

- ☑ High input Signal to Noise-Ratio
  - ☑ Ultra-high field
  - ☑ Multi-channel acquisition
- ☑ Fast acquisition
  - ☑ Variable density sampling
  - ☑ Non-Cartesian acquisition
- ☒ Fast reconstruction
  - ☒ Competitive reconstruction method
  - ☒ Exploit the wasted time of the acquisition

Outline

1. Multi-channel image reconstruction for non-Cartesian acquisition
   - State-of the art
   - Calibrationless reconstruction: Playing with the regularization
   - Experiments & Results
   - Summary
2. Online CS-MRI reconstruction
   - Problem statement: The single channel case
   - Multi-channel online reconstruction
   - Experiments & Results
   - Summary
3. Softwares

Outline

1. Multi-channel image reconstruction for non-Cartesian acquisition
   - State-of the art
   - Calibrationless reconstruction: Playing with the regularization
   - Experiments & Results
   - Summary

2. Online CS-MRI reconstruction
   - Problem statement: The single channel case
   - Multi-channel online reconstruction
   - Experiments & Results
   - Summary

3. Softwares

Multi-channel image reconstruction for non-Cartesian acquisition

This part was presented at international conferences in 2019:

Loubna El Gueddari et al. (2019a). "Calibrationless OSCAR-based image reconstruction in compressed sensing parallel MRI". In: *ISBI 2019*

Loubna El Gueddari et al. (2018). "Self-Calibrating Nonlinear Reconstruction Algorithms for Variable Density Sampling and Parallel Reception MRI". In: *IEEE SAM workshop*

This part will be submitted in a journal paper

Non-Cartesian multi-channel MR image reconstruction

State of the art method

Methods can be split in two categories:

1. Recovering a full FOV image: *Self-Calibrated reconstruction*
2. Recovering an image per channel: *Calibrationless reconstruction*

1. Self-Calibrated reconstruction:
   - Solve an inverse problem and recover a single full FOV image:

$$\widehat{\boldsymbol{x}} = \underset{\boldsymbol{x}\in\mathbb{C}^N}{\arg\min} \frac{1}{2}\sum_{\ell=1}^{L} \sigma_\ell^{-2} \|\boldsymbol{F}_\Omega \boldsymbol{S}_\ell \boldsymbol{x} - \boldsymbol{y}_\ell\|_2^2 + \lambda \|\boldsymbol{\Psi}\boldsymbol{x}\|_1 \tag{1}$$

   - Model the coil sensitivity profile $\boldsymbol{S}_\ell$ for all channels $\ell = 1, \dots, L$ [11,12]

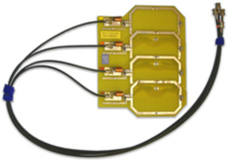

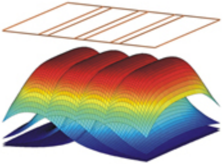

[11] Samsonov et al. 2004, *Magnetic Resonance in Medicine*.
[12] Uecker et al. 2014, *Magnetic Resonance in Medicine*.

1. Self-Calibrated reconstruction:
   - Solve an inverse problem and recover a single full FOV image:

$$\widehat{\boldsymbol{x}} = \operatorname*{arg\,min}_{\boldsymbol{x}\in\mathbb{C}^N} \frac{1}{2}\sum_{\ell=1}^{L} \sigma_\ell^{-2} \|\boldsymbol{F}_\Omega \boldsymbol{S}_\ell \boldsymbol{x} - \boldsymbol{y}_\ell\|_2^2 + \lambda \|\boldsymbol{\Psi}\boldsymbol{x}\|_1 \tag{1}$$

   - Model the coil sensitivity profile $\boldsymbol{S}_\ell$ for all channels $\ell = 1, \dots, L$ [11,12]
   - Coil sensitivity profiles are subject/scan-specific $\rightarrow$ estimated/extracted for each scan

[11] Samsonov et al. 2004, *Magnetic Resonance in Medicine*.
[12] Uecker et al. 2014, *Magnetic Resonance in Medicine*.

Non-Cartesian multi-channel MR image reconstruction

Self-Calibrated reconstruction: coil sensitivity profile estimation

- Smooth sensitivity profiles $\Longrightarrow$ can be estimated from the k-space center.

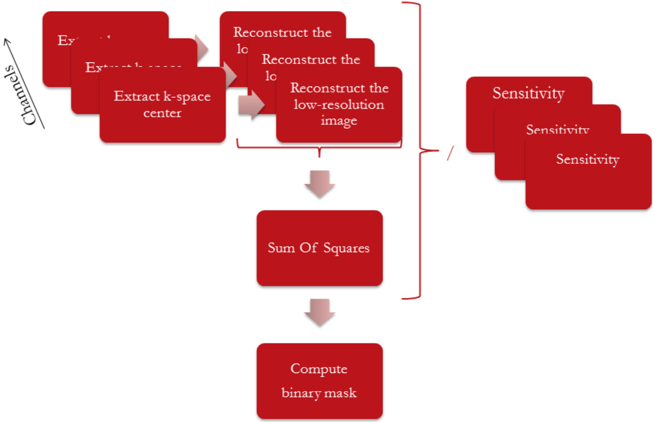

Acquisition parameters

- Field strength: 7 Tesla
- Resolution: $0.4 \times 0.4 \times 3\,\mathrm{mm}^3$
- Matrix size: 512×512
- Trajectory: Sparkling[13]
- Number of spokes (S): 34
- Acceleration/undersampling factors: 15/2.5

Cartesian Reference

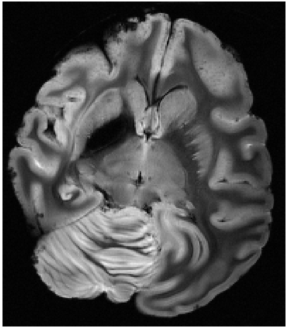

Figure: Ex-vivo baboon brain

Non-Cartesian sampling

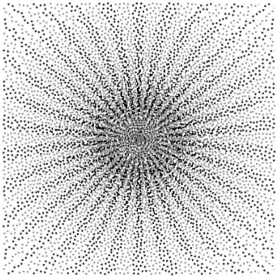

Figure: 15-fold accelerated Sparkling trajectories

[13] Lazarus et al. 2019, *Magnetic Resonance in Medicine*

- Smooth sensitivity profiles $\Longrightarrow$ can be estimated from the k-space center.

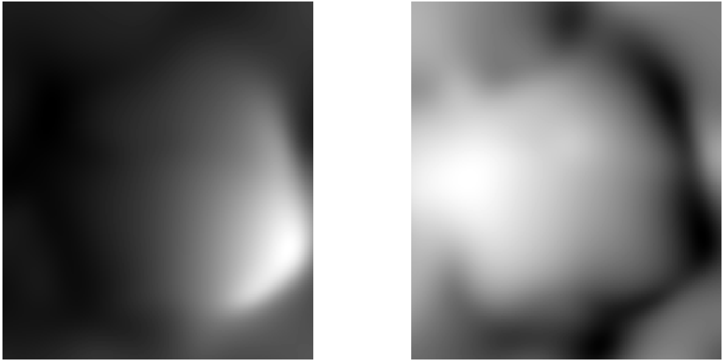

Example of two extracted sensitivity maps.

- No ground-truth is available, the performances must be measured via the recovered image.

- Smooth sensitivity profiles $\Longrightarrow$ can be estimated from the k-space center.
- No ground-truth is available, the performances must be measured via the recovered image.

Reference Proposed estimation[14] ℓ_1-ESPIRIT[15]

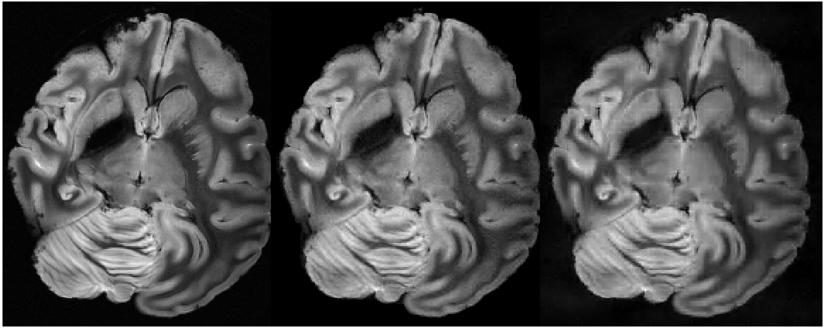

[14] El Gueddari et al. 2018, *IEEE SAM workshop*.
[15] Uecker et al. 2014, *Magnetic Resonance in Medicine*.

- Smooth sensitivity profiles $\Longrightarrow$ can be estimated from the k-space center.
- No ground-truth is available, the performances must be measured via the recovered image.

Reference | Proposed estimation[14] | ℓ_1-ESPIRIT[15]

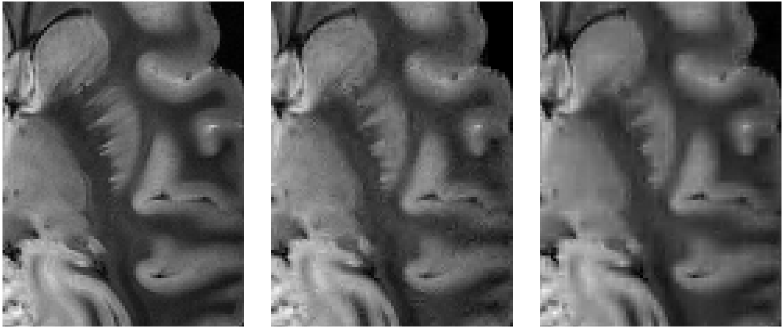

S-maps extraction: 1min | S-maps extraction: 10min

[14] El Gueddari et al. 2018, *IEEE SAM workshop*.
[15] Uecker et al. 2014, *Magnetic Resonance in Medicine*.

REFERENCE SPARKLING SPIRAL RADIAL

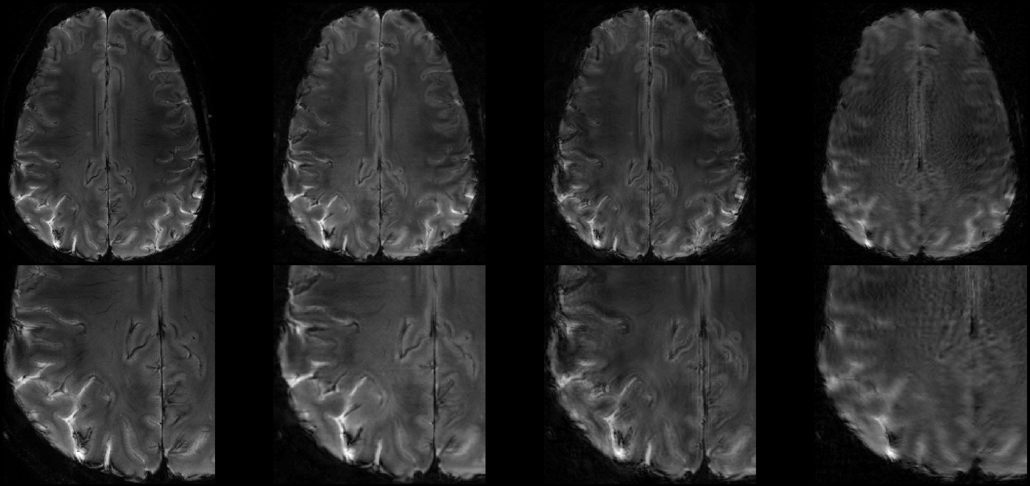

[15] Lazarus et al. 2019, *Magnetic Resonance in Medicine*

1. Self-calibrated methods, pros & cons:
    - good reconstruction performances
    - sensitivity profiles need to be set beforehand $\Longrightarrow$ pre-scan lengthen the acquisition
    - estimation must be performed during the acquisition $\Longrightarrow$ lengthen the reconstruction

1. Self-calibrated methods, pros & cons:
    - good reconstruction performances
    - sensitivity profiles need to be set beforehand $\Longrightarrow$ pre-scan lengthen the acquisition
    - estimation must be performed during the acquisition $\Longrightarrow$ lengthen the reconstruction
2. Calibrationless reconstruction
    - No longer need coil sensitivity profiles
    - Exploit redundancy across channels to impose structured sparsity

Problem statement

Calibration-less MR image reconstruction problem solved using an *analysis formulation*:

$$\widehat{\boldsymbol{X}} = \underset{\boldsymbol{X} \in \mathbb{C}^{N \times L}}{\arg\min} \frac{1}{2} \|\mathcal{F}_\Omega \boldsymbol{X} - \boldsymbol{Y}\|_2^2 + \mathcal{R}(\boldsymbol{\Psi} \boldsymbol{X}). \tag{2}$$

with:

- $\boldsymbol{Y} = [\boldsymbol{y}_1, \cdots, \boldsymbol{y}_L]$ with $\boldsymbol{y}_\ell \in \mathbb{C}^M$ the ℓ^{th} channel-specific k-space
- $\boldsymbol{X} = [\boldsymbol{x}_1, \cdots, \boldsymbol{x}_L]$ with $\boldsymbol{x}_\ell \in \mathbb{C}^N$ the ℓ^{th} channel-specific reconstructed image.
- F_Ω is the forward under-sampling Fourier operator
- $\boldsymbol{\Psi} \in \mathbb{C}^{N_\Psi \times N}$ linear operator related to a sparse decomposition
- $\mathcal{R}$ is a convex regularization term that promotes sparsity with an explicit proximity operator.

We aim to find:

$$\widehat{\boldsymbol{X}} \in \underset{\boldsymbol{X} \in \mathbb{C}^{N \times L}}{\operatorname{argmin}} \left[f(\boldsymbol{X}) + \mathcal{R}(\boldsymbol{\Psi X}) \right] \tag{3}$$

where:

- f is convex, differentiable on $\mathbb{C}^{N \times L}$ and its gradient is β-Lipschitz
- $\mathcal{R} \in \Gamma_0(\mathbb{C}^{N_\Psi \times L})$ with a closed form proximity operator[16], given by:

$$\operatorname{prox}_{\mathcal{R}}(\boldsymbol{Z}) = \underset{\boldsymbol{V} \in \mathbb{C}^{N_\Psi \times L}}{\operatorname{argmin}} \frac{1}{2} \|\boldsymbol{Z} - \boldsymbol{V}\|^2 + \mathcal{R}(\boldsymbol{V}) \tag{4}$$

Note: Those are standard assumption in optimization based image reconstruction methods.

[16] Moreau 1962, *Comptes Rendus de l'Académie des Sciences de Paris*.

Using a primal-dual optimization method proposed by Condat[17]-Vũ[18]:

Algorithm 1: Condat-Vũ algorithm

Data: $\boldsymbol{X}_0$, $\boldsymbol{Z}_0$
Result: $\boldsymbol{X}_K$, $\boldsymbol{Z}_K$
initialize $k = 0, \tau > 0, \kappa > 0$,;
while $k \leq K$ do

$$\boldsymbol{X}_{k+1} := \boldsymbol{X}_k - \tau \left(\nabla f(\boldsymbol{X}_k) + \boldsymbol{\Psi}^* \boldsymbol{Z}_k\right);$$
$$\boldsymbol{W}_{k+1} := \boldsymbol{Z}_k + \kappa \boldsymbol{\Psi} \left(2\boldsymbol{X}_{k+1} - \boldsymbol{X}_k\right);$$
$$\boldsymbol{Z}_{k+1} := \boldsymbol{W}_{k+1} - \kappa \operatorname{prox}_{g/\kappa}\left(\frac{\boldsymbol{W}_{k+1}}{\kappa}\right);$$

- if $\frac{1}{\tau} - \kappa|||\boldsymbol{\Psi}|||^2 \geq \frac{\beta}{2}$ then the algorithm weakly converges to the solution of Eq. (3).
- τ and κ hyper-parameters set as follows: $\tau := \frac{1}{\beta}$, $\kappa := \frac{\beta}{2|||\boldsymbol{\Psi}|||^2}$

[17] Condat 2013, *Journal of Optimization Theory and Applications.*
[18] Vũ 2013, *Advances in computational mathematics.*

Calibrationless reconstruction: playing with clustering regularization

Calibrationless reconstruction: playing with clustering regularization

- Clustering using the ℓ_2-norm
- Clustering using the ℓ_∞-norm

Regularizing through the Group-LASSO

Group-LASSO (GL)[19] regularization has been used in multi-task learning in different field including MRI reconstruction[20].

Ψ 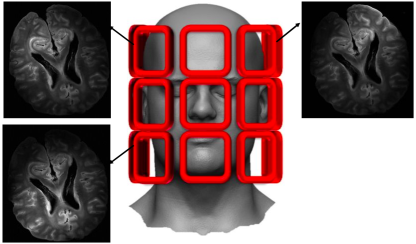 $=$ 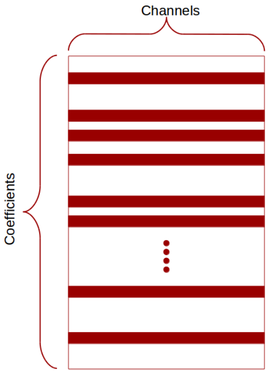

[19] Yuan and Lin 2006, *Journal of the Royal Statistical Society: Series B (Statistical Methodology)*.
[20] Majumdar and Ward 2012, *Magnetic Resonance in Medicine*.

Regularizing through the Group-LASSO

Group-LASSO (GL)[19] regularization has been used in multi-task learning in different field including MRI reconstruction[20].

The group-LASSO penalty is defined as follows:

$$\mathcal{R}_{\mathrm{GL}}(\boldsymbol{Z}) = \sum_{g \in \mathcal{G}} \|\boldsymbol{Z}_g\|_2$$

- $\mathcal{G}$ is the set of groups defining a partition of $\boldsymbol{Z}$

$\boldsymbol{Z} =$

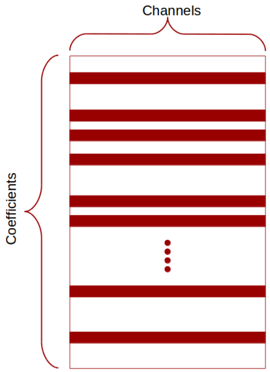

[19] Yuan and Lin 2006, *Journal of the Royal Statistical Society: Series B (Statistical Methodology)*.
[20] Majumdar and Ward 2012, *Magnetic Resonance in Medicine*.

Regularizing through the Group-LASSO

Group-LASSO (GL)[19] regularization has been used in multi-task learning in different field including MRI reconstruction[20].

The group-LASSO penalty is defined as follows:

$$\begin{aligned}\mathcal{R}_{\mathrm{GL}}(\boldsymbol{Z}) &= \|\boldsymbol{Z}\|_{2,1} \\ &= \lambda \sum_{p=1}^{N_{\Psi}} \sqrt{\sum_{\ell=1}^{L} |z_{p\ell}|^2}\end{aligned}$$

$$\boldsymbol{Z} =$$

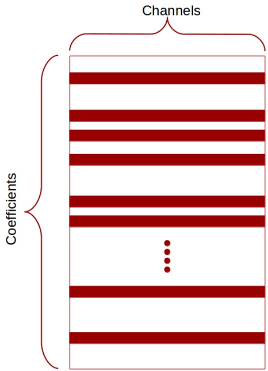

with:

- $\boldsymbol{Z} = \boldsymbol{\Psi}\boldsymbol{X}$
- λ is a positive hyper-parameter

[19] Yuan and Lin 2006, *Journal of the Royal Statistical Society: Series B (Statistical Methodology)*.
[20] Majumdar and Ward 2012, *Magnetic Resonance in Medicine*.

Regularizing through the Group-LASSO

Group-LASSO (GL)[19] regularization has been used in multi-task learning in different field including MRI reconstruction[20].

The group-LASSO penalty is defined as follows:

$$\mathcal{R}_{\mathrm{GL}}(\boldsymbol{Z}) = \|\boldsymbol{Z}\|_{2,1}$$
$$= \lambda \sum_{p=1}^{N_\Psi} \sqrt{\sum_{\ell=1}^{L} |z_{p\ell}|^2}$$

$\boldsymbol{Z} =$ 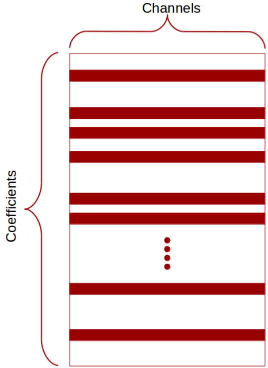

Group-LASSO regularization provides tighter recovery guarantees[21]

[19] Yuan and Lin 2006, *Journal of the Royal Statistical Society: Series B (Statistical Methodology)*.
[20] Majumdar and Ward 2012, *Magnetic Resonance in Medicine*.
[21] Chun, Adcock, and Talavage 2016, *IEEE Transactions on Medical Imaging*

Joint sparsity regularization

Group-LASSO with overlaps: k-support norm

- Relaxing the group-structure of the group-LASSO.
- Inferring the overlapping groups via the K-support norm[22].

$$
\begin{aligned}
\mathcal{R}_{\frac{1}{2}\|\cdot\|_k^{sp}} &= \frac{\lambda}{2}\|\boldsymbol{Z}\|_k^{sp} \\
&= \min\Big\{ \sum_{I \in \mathcal{G}_k} \|\boldsymbol{v}_I\|_2 : \mathrm{supp}(\boldsymbol{v}_I) \subseteq I, \sum_{I \in \mathcal{G}_k} \boldsymbol{v}_I = \boldsymbol{z} \Big\}
\end{aligned}
$$

with:

- $\mathcal{G}_k$ corresponds to the set of all subsets of $\left\{1, \ldots, N_{\boldsymbol{\Psi}} L\right\}$ of cardinality at most k.
- λ and $k \in \mathbb{N}^*$, $k \leq N_{\boldsymbol{\Psi}}$ need to be set.

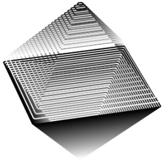

1-support unit ball

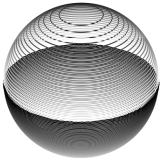

3-support unit ball

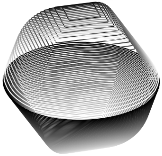

2-support unit ball in $\mathbb{R}^3$

[22] Argyriou, Foygel, and Srebro 2012, *NeurIPS*

Joint sparsity regularization
Group-LASSO with overlaps: k-support norm

- Relaxing the group-structure of the group-LASSO.
- Inferring the overlapping groups via the K-support norm[22].

$$\mathcal{R}_{\frac{1}{2}\|\cdot\|_k^{sp}} = \frac{\lambda}{2}\|\boldsymbol{Z}\|_k^{sp}$$
$$= \min\{\sum_{I\in\mathcal{G}_k} \|\boldsymbol{v}_I\|_2 : \mathrm{supp}(\boldsymbol{v}_I) \subseteq I, \sum_{I\in\mathcal{G}_k} \boldsymbol{v}_I = \boldsymbol{z}\}$$

- Let $\|\cdot\|$ be a norm, its dual norm $\|\cdot\|_*$ is defined as:

$$\|z\| = \sup\left\{x \in \mathbb{R}^N \langle z, x\rangle \quad | \quad \|x\| \leq 1\right\}$$

- Fairly simple dual norm:

$$\|\boldsymbol{u}\|_k^{sp^\star} := \left(\sum_{i=1}^{k}(|\boldsymbol{u}|_\downarrow)_i^2\right)^{\frac{1}{2}}$$

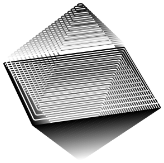

1-support unit ball

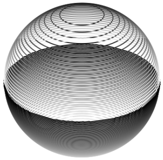

3-support unit ball

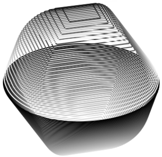

2-support unit ball in $\mathbb{R}^3$

From Hölder's inequality the dual of an ℓ_p norm is an ℓ_q norm with $p^{-1} + q^{-1} = 1$

[22] Argyriou, Foygel, and Srebro 2012, *NeurIPS*

Joint sparsity regularization

Octagonal Shrinkage and Clustering Algorithm for Regression

- Inferring the structure via a pairwise ℓ_∞ norm.
- OSCAR regularization[23]:

$$\mathcal{R}_{\text{c-OSCAR}}(\boldsymbol{Z}) = \sum_{p=1}^{N_\Psi} \lambda \left[\sum_{\ell=1}^{L} |z_{pj}| + \gamma \sum_{\ell<k} \max\{|z_{p\ell}|, |z_{pk}|\} \right]$$

$$= \sum_{p=1}^{N_\Psi} \lambda \left[\sum_{\ell=1}^{L} (\gamma(\ell-1)+1) \, |z_{p\ell}|_{\downarrow} \right]$$

where:

- $\boldsymbol{Z}_{\downarrow} \in \mathbb{C}^{N_\Psi \times L}$ the wavelet coefficients sorted in decreasing order, i.e.: $\forall p \in \mathbb{N}, |z_{p1}| \leq \cdots \leq |z_{pL}|$.
- λ and γ are some positive hyper-parameters that need to be set

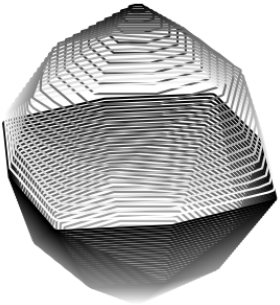

Figure: OSCAR's unit ball

Note: OSCAR has an explicit proximity operator

[23] Bondell and Reich 2008, *Biometrics*.

Experimental set-up

Sequence parameters:

- Ex-vivo human brain
- 7T Siemens Scanner
- 1Tx/32Rx Nova coil
- GRE Sparkling trajectory
- 0.390 x 0.390 x 1.5 m^3 resolution
- Acceleration factor of 20 in time
- Under-sampling factor of 2.5
- $\boldsymbol{\Psi}$: Daubechies 4 transform

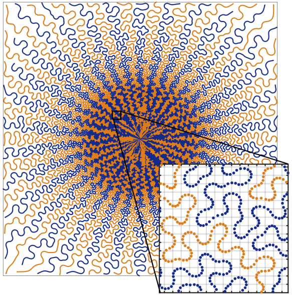

Figure: Sparkling trajectory

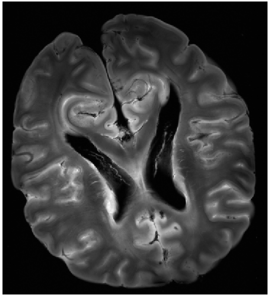

Figure: Ex-vivo Human brain

Hyper-parameters set using a grid-search procedure to maximize the SSIM score.
Cartesian scan 512×512 was acquired and used for reference.

Results

Similarity score

	iFT	ℓ_1-ESPIRIT[24]	p-LORAKS[25]	group-LASSO[26]	c-OSCAR[27]	k-support norm
SSIM	0.884	0.885	0.753	0.897	0.901	0.900
pSNR	28.25	26.48	25.52	28.59	29.77	30.29
NRMSE	0.1911	0.2276	0.2536	0.1859	0.1604	0.1510

[24] Uecker et al. 2014, *Magnetic Resonance in Medicine*.
[25] Haldar and Zhuo 2016, *Magnetic resonance in medicine*.
[26] Majumdar and Ward 2012, *Magnetic Resonance in Medicine*.
[27] El Gueddari et al. 2019a, *ISBI 2019*.

Results

Magnitude images

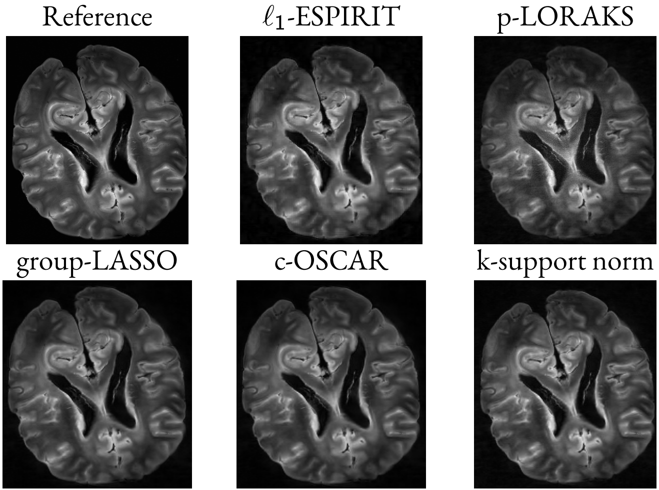

Results

Magnitude images

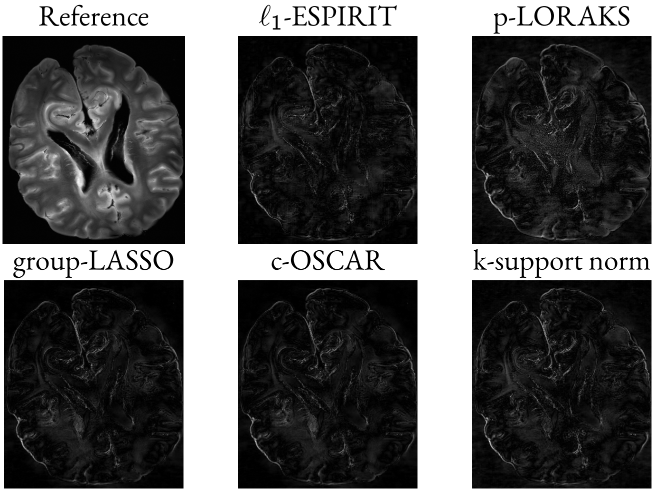

Results

Magnitude images

ℓ_1-ESPIRIT

p-LORAKS

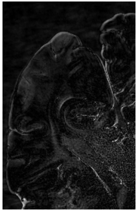

group-LASSO

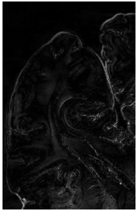

c-OSCAR

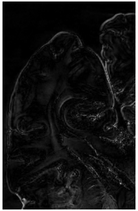

k-support norm

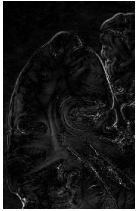

Results

Phase images

Reference

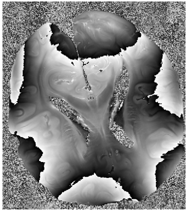

ℓ_1-ESPIRIT

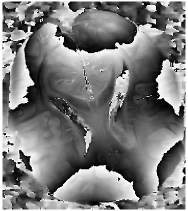

p-LORAKS

group-LASSO

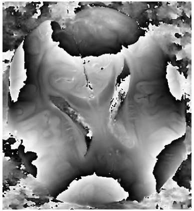

OSCAR

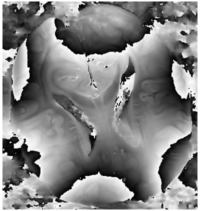

k-support norm

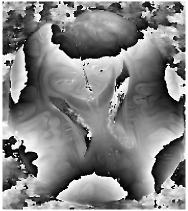

Partial Summary

Summary:

- Investigate two classes of MR image reconstruction methods for non-Cartesian acquisition
- Propose a simple, versatile, yet efficient algorithm to extract the coil sensitivity profile information
- Investigate new penalization for calibrationless reconstruction

$\rightarrow$ How can we speed-up the reconstruction.

Outline

Online CS-MRI reconstruction

This part was presented at international conferences in 2019:

Loubna El Gueddari et al. (2019b). "Online compressed sensing MR image reconstruction for high resolution T2* imaging". In: *Proceedings of the 27th Annual Meeting of ISMRM*, p. 4679

Loubna El Gueddari et al. (2019c). "Online MR image reconstruction for compressed sensing acquisition in T2* imaging.". In: *Wavelets: Applications in Signal and Image Processing XVIII*

Speeding-up the reconstruction

- Structural MRI acquisition is segmented in time

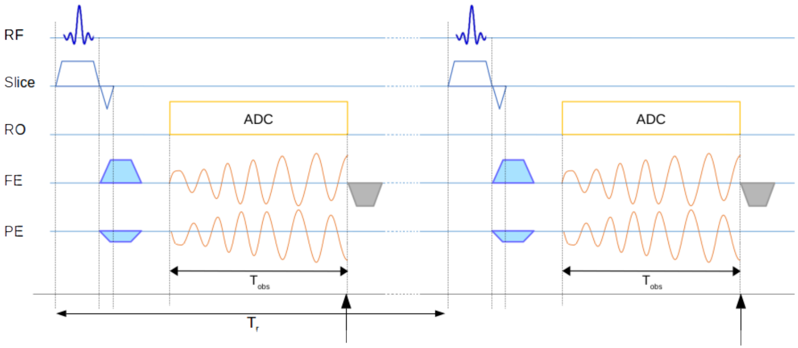

Speeding-up the reconstruction

- Structural MRI acquisition is segmented in time

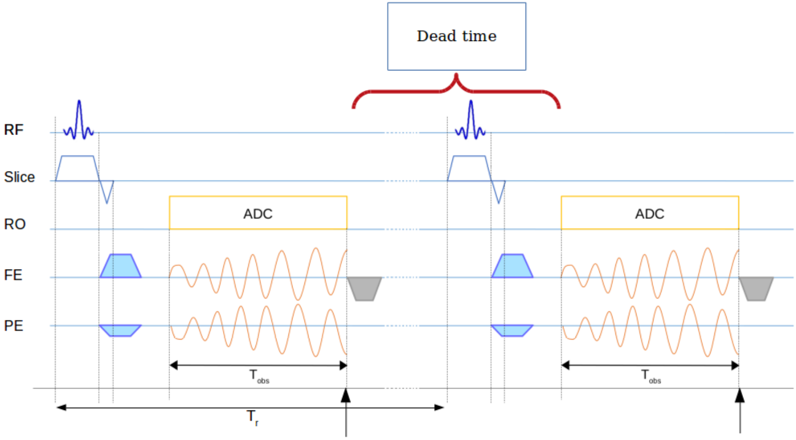

Online CS-MRI reconstruction

Single-channel receiver case

- Multi-shot acquisition: $\forall i \in \{1, \dots, S\}$, collect data $\boldsymbol{y}_i$ over Γ_i support with $|\Gamma_i| = C$

Online CS-MRI reconstruction

Single-channel receiver case

- Multi-shot acquisition: $\forall i \in \{1, \dots, S\}$, collect data $\boldsymbol{y}_i$ over Γ_i support with $|\Gamma_i| = C$
- Define the kth mini-batch as $\Omega_k = \cup_{i=1}^{k} \Gamma_i$
- Solve partial image reconstruction:

$$\forall k \in \{1, \dots, S\}, \qquad \widehat{\boldsymbol{x}}^k = \underset{\boldsymbol{x} \in \mathbb{C}^N}{\arg\min} \frac{S}{2k} \|\boldsymbol{F}_{\Omega_k} \boldsymbol{x} - \boldsymbol{y}_{\Omega_k}\|_{\mathrm{F}}^2 + \lambda \|\boldsymbol{\Psi} \boldsymbol{x}\|_1, \tag{5}$$

Online time constraints:

$$\boxed{n_b \times T_{\mathrm{it}} \approx b_s \times \mathrm{TR}.}$$

with:

- $\mathcal{F}_{\Omega_k}$: undersampled Fourier operator over Ω_k
- $\boldsymbol{y}_{\Omega_k}$: complex-valued k-space measurements over Ω_k
- $\widehat{\boldsymbol{x}}^k$: estimated MR image from incomplete data $\boldsymbol{y}_{\Omega_k}$

- The problem is convex $\rightarrow$ final solution does not depend on the initialization.

Online optimization algorithm
Single-channel receiver case

To solve Pb (5), we adapted the Condat-Vũ algorithm to the online framework.

Algorithm 1: Online primal-dual optimization algorithm.

initialize $k = b_s$, $\boldsymbol{x}^0, \boldsymbol{z}^0$;
while $k \leq S$ do
  $\tau_k = 1/\beta_k$;
  $\kappa_k = \beta_k / (2|||\boldsymbol{\Psi}|||^2)$;
  for $t = 1, 2, \dots, n_b$ do
    $\boldsymbol{x}_t^k = \boldsymbol{x}_{t-1}^k - \tau_k \left(\nabla f_{\Omega_k}(\boldsymbol{x}_{t-1}^k) + \boldsymbol{\Psi}^* \boldsymbol{z}_{t-1}^k \right)$;
    $\boldsymbol{w}_t^k = \boldsymbol{z}_{t-1}^k + \kappa_k \boldsymbol{\Psi} \left(2\boldsymbol{x}_t^k - \boldsymbol{x}_{t-1}^k \right)$;
    $\boldsymbol{z}_t^k = \boldsymbol{w}_t^k - \kappa_k \operatorname{prox}_{g/\kappa_k} \left(\boldsymbol{w}_t^k / \kappa_k \right)$;
  $(\boldsymbol{x}_0^{k+b_s}, \boldsymbol{z}_0^{k+b_s}) \leftarrow (\boldsymbol{x}_{n_b}^k, \boldsymbol{z}_{n_b}^k)$;
  $k \leftarrow k + b_s$;

To solve Pb (5), we adapted the Condat-Vũ algorithm to the online framework.

Algorithm 1: Online primal-dual optimization algorithm.

initialize $k = b_s$, $\boldsymbol{x}^0, \boldsymbol{z}^0$;

while $k \leq S$ do

- $\tau_k = 1/\beta_k$;
- $\kappa_k = \beta_k / (2|||\boldsymbol{\Psi}|||^2)$;
- for $t = 1, 2, \dots, n_b$ do
  - $\boldsymbol{x}_t^k = \boldsymbol{x}_{t-1}^k - \tau_k \left(\nabla f_{\Omega_k}(\boldsymbol{x}_{t-1}^k) + \boldsymbol{\Psi}^* \boldsymbol{z}_{t-1}^k \right)$;
  - $\boldsymbol{w}_t^k = \boldsymbol{z}_{t-1}^k + \kappa_k \boldsymbol{\Psi} \left(2\boldsymbol{x}_t^k - \boldsymbol{x}_{t-1}^k \right)$;
  - $\boldsymbol{z}_t^k = \boldsymbol{w}_t^k - \kappa_k \operatorname{prox}_{g/\kappa_k} \left(\boldsymbol{w}_t^k / \kappa_k \right)$;
- $(\boldsymbol{x}_0^{k+b_s}, \boldsymbol{z}_0^{k+b_s}) \leftarrow (\boldsymbol{x}_{n_b}^k, \boldsymbol{z}_{n_b}^k)$;
- $k \leftarrow k + b_s$;

Primal variable

To solve Pb (5), we adapted the Condat-Vũ algorithm to the online framework.

Algorithm 1: Online primal-dual optimization algorithm.

initialize $k = b_s$, $\boldsymbol{x}^0, \boldsymbol{z}^0$;

while $k \leq S$ do

- $\tau_k = 1/\beta_k$;
- $\kappa_k = \beta_k / (2|||\boldsymbol{\Psi}|||^2)$;
- for $t = 1, 2, \dots, n_b$ do
  - $\boldsymbol{x}_t^k = \boldsymbol{x}_{t-1}^k - \tau_k \left(\nabla f_{\Omega_k}(\boldsymbol{x}_{t-1}^k) + \boldsymbol{\Psi}^* \boldsymbol{z}_{t-1}^k \right)$;
  - $\boldsymbol{w}_t^k = \boldsymbol{z}_{t-1}^k + \kappa_k \boldsymbol{\Psi} \left(2\boldsymbol{x}_t^k - \boldsymbol{x}_{t-1}^k \right)$;
  - $\boldsymbol{z}_t^k = \boldsymbol{w}_t^k - \kappa_k \operatorname{prox}_{g/\kappa_k} \left(\boldsymbol{w}_t^k / \kappa_k \right)$;
- $(\boldsymbol{x}_0^{k+b_s}, \boldsymbol{z}_0^{k+b_s}) \leftarrow (\boldsymbol{x}_{n_b}^k, \boldsymbol{z}_{n_b}^k)$;
- $k \leftarrow k + b_s$;

Dual variable

Online optimization algorithm

Single-channel receiver case

To solve Pb (5), we adapted the Condat-Vũ algorithm to the online framework.

Algorithm 1: Online primal-dual optimization algorithm.

initialize $k = b_s,\ \boldsymbol{x}^0, \boldsymbol{z}^0$;

while $k \leq S$ do

- $\tau_k = 1/\beta_k$;
- $\kappa_k = \beta_k/(2|||\boldsymbol{\Psi}|||^2)$;
- for $t = 1, 2, \ldots, n_b$ do
  - $\boldsymbol{x}_t^k = \boldsymbol{x}_{t-1}^k - \tau_k \left(\nabla f_{\Omega_k}(\boldsymbol{x}_{t-1}^k) + \boldsymbol{\Psi}^* \boldsymbol{z}_{t-1}^k\right)$;
  - $\boldsymbol{w}_t^k = \boldsymbol{z}_{t-1}^k + \kappa_k \boldsymbol{\Psi} \left(2\boldsymbol{x}_t^k - \boldsymbol{x}_{t-1}^k\right)$;
  - $\boldsymbol{z}_t^k = \boldsymbol{w}_t^k - \kappa_k \operatorname{prox}_{g/\kappa_k} \left(\boldsymbol{w}_t^k/\kappa_k\right)$;
- $(\boldsymbol{x}_0^{k+b_s}, \boldsymbol{z}_0^{k+b_s}) \leftarrow (\boldsymbol{x}_{n_b}^k, \boldsymbol{z}_{n_b}^k)$;
- $k \leftarrow k + b_s$;

Primal gradient step

Online optimization algorithm

Single-channel receiver case

To solve Pb (5), we adapted the Condat-Vũ algorithm to the online framework.

Algorithm 1: Online primal-dual optimization algorithm.

initialize $k = b_s$, $\boldsymbol{x}^0, \boldsymbol{z}^0$;

while $k \leq S$ do

- $\tau_k = 1/\beta_k$;
- $\kappa_k = \beta_k / (2|||\boldsymbol{\Psi}|||^2)$;
- for $t = 1, 2, \dots, n_b$ do
  - $\boldsymbol{x}_t^k = \boldsymbol{x}_{t-1}^k - \tau_k \left(\nabla f_{\Omega_k}(\boldsymbol{x}_{t-1}^k) + \boldsymbol{\Psi}^* \boldsymbol{z}_{t-1}^k \right)$;
  - $\boldsymbol{w}_t^k = \boldsymbol{z}_{t-1}^k + \kappa_k \boldsymbol{\Psi} \left(2\boldsymbol{x}_t^k - \boldsymbol{x}_{t-1}^k \right)$;
  - $\boldsymbol{z}_t^k = \boldsymbol{w}_t^k - \kappa_k \operatorname{prox}_{g/\kappa_k} \left(\boldsymbol{w}_t^k / \kappa_k \right)$;
- $(\boldsymbol{x}_0^{k+b_s}, \boldsymbol{z}_0^{k+b_s}) \leftarrow (\boldsymbol{x}_{n_b}^k, \boldsymbol{z}_{n_b}^k)$;
- $k \leftarrow k + b_s$;

Dual proximal step

To solve Pb (5), we adapted the Condat-Vũ algorithm to the online framework.

Algorithm 1: Online primal-dual optimization algorithm.

initialize $k = b_s,\ \boldsymbol{x}^0, \boldsymbol{z}^0$;

while $k \leq S$ do

- $\tau_k = 1/\beta_k$;
- $\kappa_k = \beta_k / (2|||\boldsymbol{\Psi}|||^2)$;
- for $t = 1, 2, \dots, n_b$ do

$$\left.\begin{aligned} \boldsymbol{x}_t^k &= \boldsymbol{x}_{t-1}^k - \tau_k \left(\nabla f_{\Omega_k}(\boldsymbol{x}_{t-1}^k) + \boldsymbol{\Psi}^* \boldsymbol{z}_{t-1}^k\right); \\ \boldsymbol{w}_t^k &= \boldsymbol{z}_{t-1}^k + \kappa_k \boldsymbol{\Psi} \left(2\boldsymbol{x}_t^k - \boldsymbol{x}_{t-1}^k\right); \\ \boldsymbol{z}_t^k &= \boldsymbol{w}_t^k - \kappa_k \operatorname{prox}_{g/\kappa_k}\left(\boldsymbol{w}_t^k / \kappa_k\right); \\ (\boldsymbol{x}_0^{k+b_s}, \boldsymbol{z}_0^{k+b_s}) &\leftarrow (\boldsymbol{x}_{n_b}^k, \boldsymbol{z}_{n_b}^k); \end{aligned}\right\} \text{Condat-Vũ sequence}$$

- $k \leftarrow k + b_s$;

Online optimization algorithm

Single-channel receiver case

To solve Pb (5), we adapted the Condat-Vũ algorithm to the online framework.

Algorithm 1: Online primal-dual optimization algorithm.

initialize $k = b_s,\ \boldsymbol{x}^0, \boldsymbol{z}^0$;

while $k \leq S$ do

  $\tau_k = 1/\beta_k$;

  $\kappa_k = \beta_k / (2 |||\boldsymbol{\Psi}|||^2)$;

  for $t = 1, 2, \ldots, n_b$ do

    $\boldsymbol{x}_t^k = \boldsymbol{x}_{t-1}^k - \tau_k \left(\nabla f_{\Omega_k}(\boldsymbol{x}_{t-1}^k) + \boldsymbol{\Psi}^* \boldsymbol{z}_{t-1}^k\right)$;

    $\boldsymbol{w}_t^k = \boldsymbol{z}_{t-1}^k + \kappa_k \boldsymbol{\Psi} \left(2\boldsymbol{x}_t^k - \boldsymbol{x}_{t-1}^k\right)$;

    $\boldsymbol{z}_t^k = \boldsymbol{w}_t^k - \kappa_k \operatorname{prox}_{g/\kappa_k}\left(\boldsymbol{w}_t^k / \kappa_k\right)$;

  $(\boldsymbol{x}_0^{k+b_s}, \boldsymbol{z}_0^{k+b_s}) \leftarrow (\boldsymbol{x}_{n_b}^k, \boldsymbol{z}_{n_b}^k)$;

  $k \leftarrow k + b_s$;

Warm restart

To solve Pb (5), we adapted the Condat-Vũ algorithm to the online framework.

Algorithm 1: Online primal-dual optimization algorithm.

initialize $k = b_s,\ \boldsymbol{x}^0, \boldsymbol{z}^0$;

while $k \leq S$ do

$\quad \tau_k = 1/\beta_k$;

$\quad \kappa_k = \beta_k/(2|||\boldsymbol{\Psi}|||^2)$;

$\quad$ for $t = 1, 2, \ldots, n_b$ do

$$\boldsymbol{x}_t^k = \boldsymbol{x}_{t-1}^k - \tau_k \left(\nabla f_{\Omega_k}(\boldsymbol{x}_{t-1}^k) + \boldsymbol{\Psi}^* \boldsymbol{z}_{t-1}^k\right);$$

$$\boldsymbol{w}_t^k = \boldsymbol{z}_{t-1}^k + \kappa_k \boldsymbol{\Psi} \left(2\boldsymbol{x}_t^k - \boldsymbol{x}_{t-1}^k\right);$$

$$\boldsymbol{z}_t^k = \boldsymbol{w}_t^k - \kappa_k \operatorname{prox}_{g/\kappa_k} \left(\boldsymbol{w}_t^k/\kappa_k\right);$$

$\quad (\boldsymbol{x}_0^{k+b_s}, \boldsymbol{z}_0^{k+b_s}) \leftarrow (\boldsymbol{x}_{n_b}^k, \boldsymbol{z}_{n_b}^k)$;

$\quad k \leftarrow k + b_s$;

Concatenate batches

Acquisition parameters for prospective CS

Single-channel receiver case

Acquisition parameters

- Field strength: 7 Tesla
- Repetition Time (TR): 550 ms
- Echo Time (TE): 30 ms
- Field of View: 20.4 cm
- Resolution: $0.4 \times 0.4 \times 3\,\mathrm{mm}^3$
- Matrix size: 512×512
- Trajectory: Sparkling[30]
- Number of spokes (S): 34
- Acceleration/undersampling factors: 15/2.5

Cartesian Reference

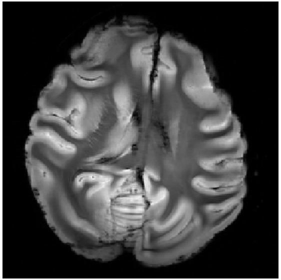

Figure: Ex-vivo baboon brain

Non-Cartesian sampling

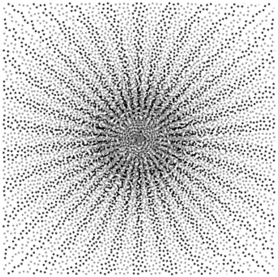

Figure: 15-fold accelerated Sparkling trajectories

[30] Lazarus et al. 2019, *Magnetic Resonance in Medicine*

Reconstruction parameters for online image processing

Single-channel receiver case

Online processing constraints

$$\boxed{n_b \times T_{\text{it}} \approx b_s \times \text{TR}.}$$

- Fourier Transform: GPU NUFFT[31]
- Time per iteration: $T_{\text{it}} \simeq 78.2 \pm 8.9$ ms
- Nb. shots/mini-batch: $b_s \in \{1, 2, 17, 34\}$
- Nb. iterations/mini-batch: $n_b \in \{5, 11, 93, 200\}$

Regularization term

- Sparse transform: 2D decimated Symmlet-8 WT
- Hyper-parameter: λ retrospectively tuned

[31] Lin 2018, *Journal of Imaging*

Non-Cartesian online CS-MR image reconstruction

Single-channel receiver case

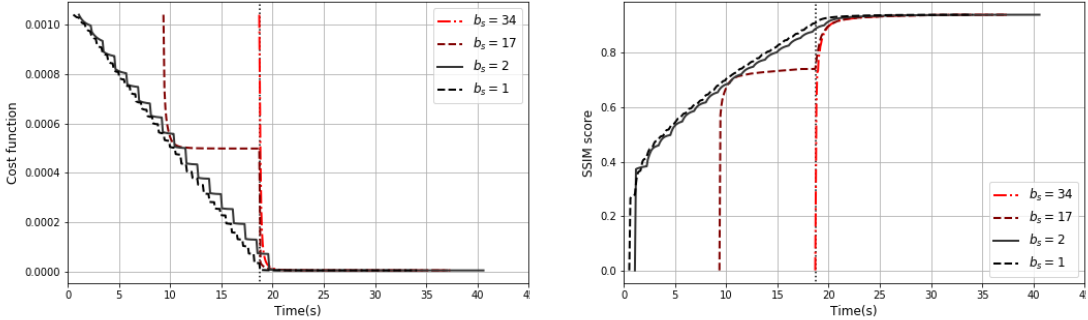

Figure: Evolution of the global cost function (left) and SSIM score (right) over time.

Non-Cartesian online CS-MR image reconstruction

Single-channel receiver case

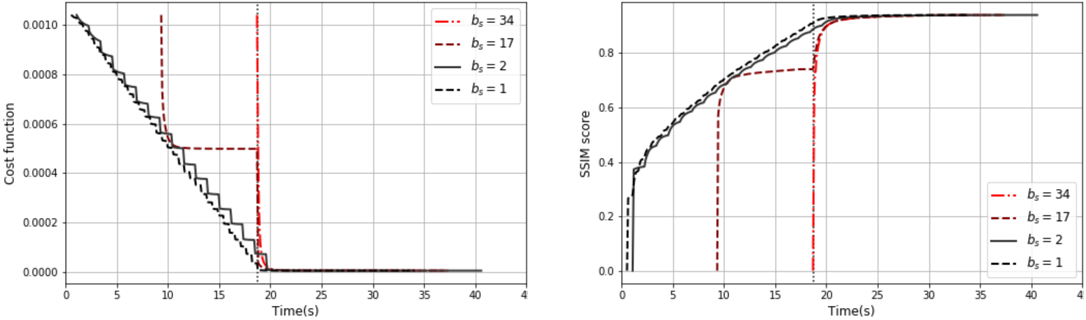

Figure: Evolution of the global cost function (left) and SSIM score (right) over time.

$\Longrightarrow$ The smaller the mini-batch size, the sooner and better the image solution.

Non-Cartesian online CS-MR image reconstruction

Single-channel receiver case

Evolution of the output $\widehat{\boldsymbol{x}}_k$ over the acquisition, mini-batch size of 1.

Figure: Collected spokes over time

Figure: Evolution of $\widehat{\boldsymbol{x}}_k$ over time

Extension to the multi-channel acquisition

Reconstruction method for multi-channel non-Cartesian acquisitions:

1. Self-Calibrated reconstruction
   - ☑ Provides good reconstruction
   - ☒ Requires the coil sensitivity maps estimation
   - ☒ Gradient-Lipschitz constant depends on the sensitivity profile estimation
2. Calibrationless reconstruction
   - ☑ Slightly better reconstruction
   - ☑ Does not rely on coil sensitivity profiles
   - ☑ Lipschitz constant only depends on the sampling pattern
   - → More suited for online reconstruction

Extension to the multi-channel acquisition

- Rely on calibrationless reconstruction

$$\widehat{\boldsymbol{X}}^k = \underset{\boldsymbol{X} \in \mathbb{C}^{N \times L}}{\arg\min} \frac{1}{2} \| \mathcal{F}_{\Omega_k} \boldsymbol{X} - \boldsymbol{Y}_{\Omega_k} \|_2^2 + \mathcal{R}(\boldsymbol{\Psi} \boldsymbol{X}). \tag{6}$$

- with OSCAR as regularization:

$$\boldsymbol{Z} = \boldsymbol{\Psi} \boldsymbol{X}, \quad \mathcal{R}_{\text{b-OSCAR}}(\boldsymbol{Z}) = \sum_{b=1}^{B} \sum_{j=1}^{P_b} \left(\sum_{\ell=1}^{L} \lambda |z_{\ell,b,j}| + \gamma \sum_{\ell' < \ell} \max\{|z_{\ell,b,j}|, |z_{\ell',b,j}|\} \right), \tag{7}$$
$$\lambda > 0, \ \gamma > 0.$$

Acquisition parameters for prospective CS

Multi-channel receiver case

Acquisition parameters

- Field strength: 7 Tesla
- Nb of coils (L): 32
- Repetition Time (TR): 550 ms
- Field of View: 20.4 cm
- Resolution: $0.4 \times 0.4 \times 1.5$ mm^3
- Trajectory: Sparkling[32]
- Number of spokes (S): 34
- Acceleration/undersampling factors: 15/2.5

Cartesian reference

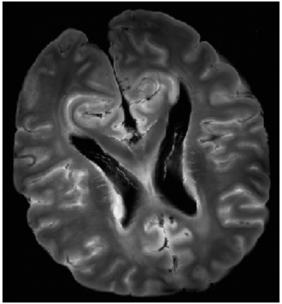

Figure: Ex-vivo human brain

Non-Cartesian sampling

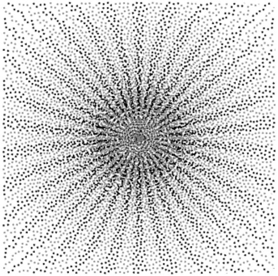

Figure: 15-fold accelerated Sparkling trajectories

[32] Lazarus et al. 2019, *Magnetic Resonance in Medicine*

Reconstruction parameters for online image processing

Multi-channel receiver case

Online processing constraints

$$\boxed{n_b \times T_{\text{it}} \approx b_s \times \text{TR}.}$$

- Fourier Transform: GPU NUFFT[33]
- Time per iteration: $T_{\text{it}} \simeq 4.29 \pm 0.111$ s
- Nb. shots/mini-batch: $b_s \in \{17,\ 34\}$
- Nb. iterations/mini-batch: $n_b \in \{1,\ 200\}$

Regularization term

- Sparse transform: 2D decimated Symmlet-8 WT
- Hyper-parameter: (λ, γ) retrospectively tuned

[33] Lin 2018, *Journal of Imaging*

Results: Prospective non-Cartesian reconstruction

Online multi-channel reconstruction

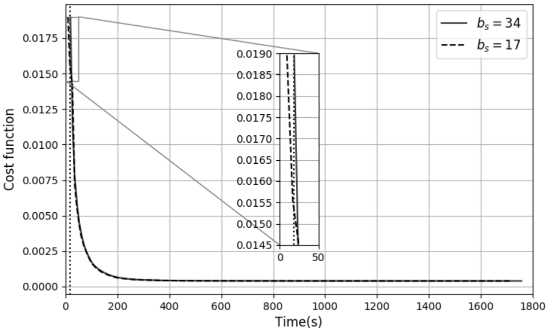

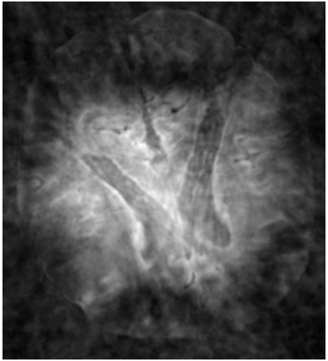

Figure: Evolution of the global cost function (left) and estimated image obtained by the end of acquisition.

Which term contributes the most to the global cost function?

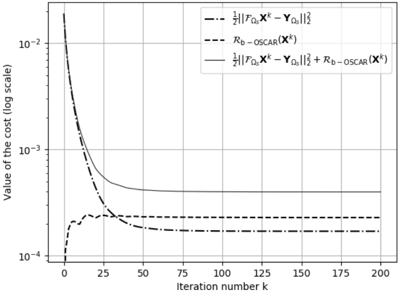

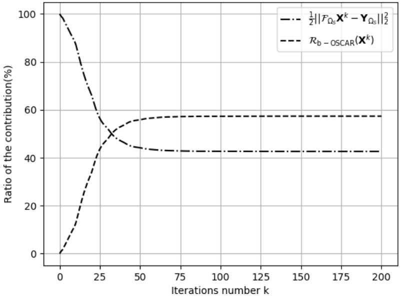

Profiling computation time

Online multi-channel reconstruction

Which term contributes the most to the global cost function?

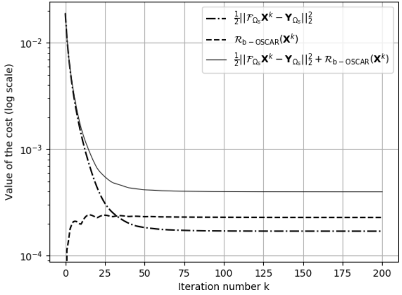

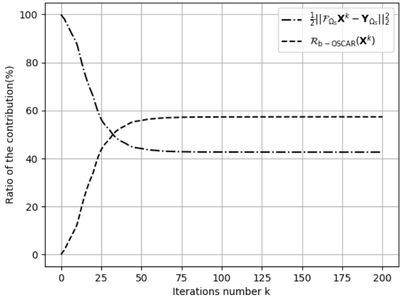

	Gradient step	Proximity op. step	Linear Operator		Total time per iteration
			direct	adjoint	
$S = 34$	750 ms $\pm$ 32.2 ms	847 ms $\pm$ 17.9 ms	998 ms $\pm$ 15.8 ms	667 ms $\pm$ 16.2 ms	4.29 s $\pm$ 111 ms

Which term contributes the most to the global cost function?

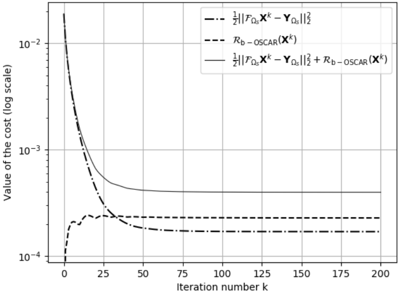

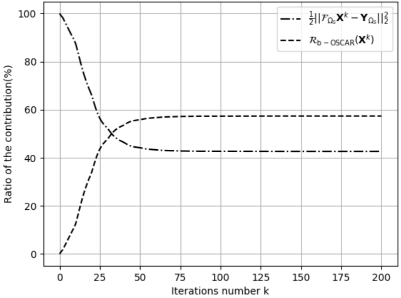

- The contribution of the data fidelity term is predominant during the first iterations.
- The gradient step only takes a quarter of computing time per iteration.

$\Longrightarrow$ During acquisition: minimizing only the smooth term.

Algorithm 1: A fast method for online CS+PI calibration-less reconstruction

initialize $k = b_s, \boldsymbol{X}^0, \boldsymbol{Z}^0$;
while $k \leq S - b_s$ do
  for $t = 1, 2, \dots, n_b$ do
    $\boldsymbol{X}_t^k = \boldsymbol{X}_{t-1}^k - \left(\nabla f_{\Omega_k}(\boldsymbol{X}_{t-1}^k)\right) / \beta_k$;
  $\boldsymbol{X}_0^{k+b_s} \leftarrow \boldsymbol{X}_{n_b}^k$;
  $k \leftarrow k + b_s$;

Adaptive Gradient step

$\boldsymbol{Z}_0^S \leftarrow \boldsymbol{\Psi}\boldsymbol{X}_0^S$;
$\tau \leftarrow 1/\beta_S$;
$\kappa = \beta_S/(2|||\boldsymbol{\Psi}|||^2)$;
for $t = 1, 2, \dots, 200$ do
  $\boldsymbol{X}_t^S = \boldsymbol{X}_{t-1}^S - \tau\left(\nabla f_{\Omega_S}(\boldsymbol{X}_{t-1}^S) + \boldsymbol{\Psi}^* \boldsymbol{Z}_{t-1}^S\right)$;
  $\boldsymbol{W}_t^S = \boldsymbol{Z}_{t-1}^S + \kappa\boldsymbol{\Psi}\left(2\boldsymbol{X}_t^S - \boldsymbol{X}_{t-1}^S\right)$;
  $\boldsymbol{Z}_t^S = \boldsymbol{W}_t^S - \kappa \operatorname{prox}_{g/\kappa}\left(\boldsymbol{W}_t^S/\kappa\right)$;

Solving calibration-less problem via Condat-Vũ algorithm

- Minimizing only the data-fidelity term allowed us to reduce the mini-batch size to 2 shots.

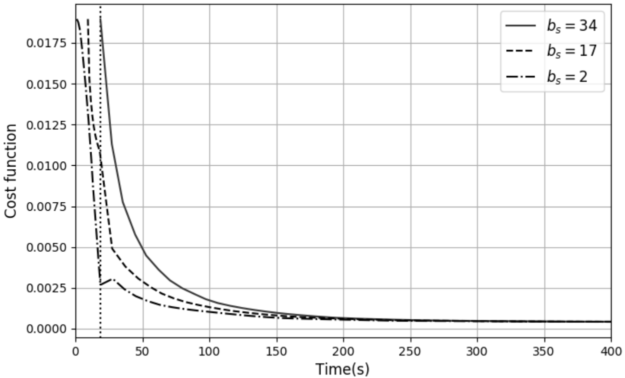

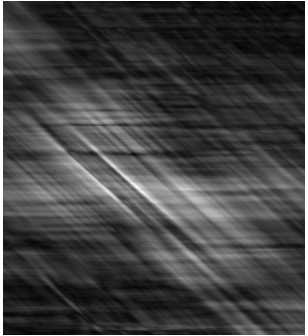

With the online trick

Online calibration-less CS-PI reconstruction

Multi-channel receiver case

- Comparison with the fully online framework

First approach

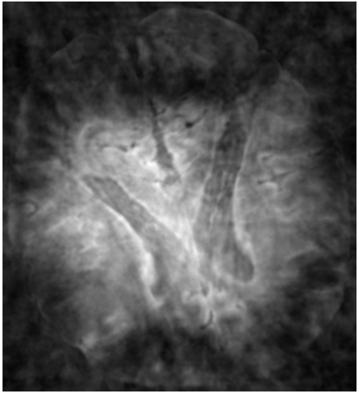

With the online trick

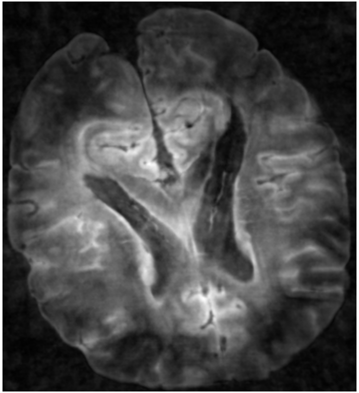

Online calibration-less CS-PI reconstruction

Multi-channel receiver case

- Recovered solution at convergence

Reference

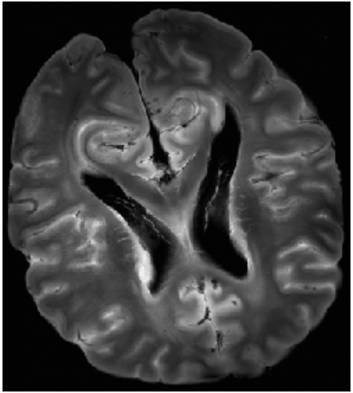

Calibrationless reconstruction

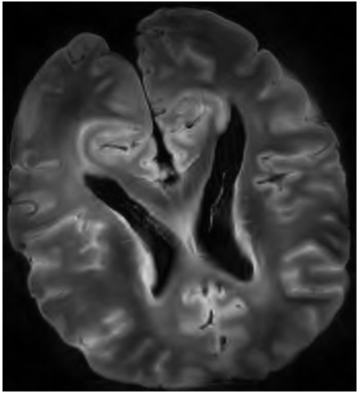

Online reconstruction

Partial summary

- Proposed an online reconstruction approach for MR image reconstruction
- Small batches allow to achieve high image quality by the end of acquisition.
- Proposed a calibration-less approach to solve the online multi-channel reconstruction.
- For both single & multi-channel reconstruction has been speed up.

Toward fast high-resolution imaging in clinical practice

- ☑ High input Signal to Noise-Ratio
  - ☑ Ultra-high field
  - ☑ Multi-channel acquisition
- ☑ Fast acquisition
  - ☑ Variable density sampling
  - ☑ Non-Cartesian acquisition
- ☑ Fast reconstruction
  - ☑ Competitive reconstruction method
  - ☑ Exploit the wasted time of the acquisition

→ Implementation on the system

Outline

1. Multi-channel image reconstruction for non-Cartesian acquisition
   - State-of the art
   - Calibrationless reconstruction: Playing with the regularization
   - Experiments & Results
   - Summary
2. Online CS-MRI reconstruction
   - Problem statement: The single channel case
   - Multi-channel online reconstruction
   - Experiments & Results
   - Summary
3. Softwares

Image reconstruction

Python package for image reconstruction: PYthon Sparse data Analysis Package (pySAP)

- Free open source python package
- With a dedicated plugin for MRI reconstruction [34]
- Unit-tested & Continuous integration
- Examples
- Documentation

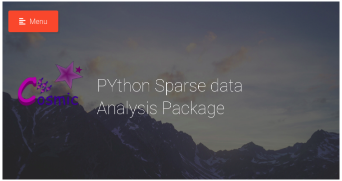

[34] El Gueddari et al. 2020, *ISMRM workshop on Data Sampling*

- Communication with the Scanner is performed using the Gadgetron [35] framework
  - Free & open-source
  - Flexible: independent of operating system
  - Vendor independent software
  - Modular: Modules can be shared across scanners
  - Can be used with various programming languages

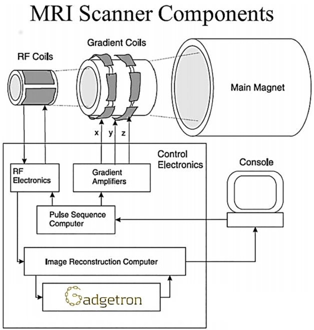

[35] Hansen and Sørensen 2013, *Magnetic resonance in medicine*

Conclusion

- The goal of this work was to :
  - Improve the reconstruction quality in multi-channel non-Cartesian high-resolution imaging
  - Provide a feedback during the scan
  - Implement and share the code
- Future work:
  - Hyper-parameters set-up
  - Faster optimization method
- Major bottleneck remains the computation time & memory footprint in 3D high-resolution imaging

$\rightarrow$ stochastic implementation

Publications I

Articles in Peer-Reviewed Journals

Loubna El Gueddari, Emilie Chouzenoux, Alexandre Vignaud and Philippe Ciuciu. *Calibrationless parallel imaging Compressed Sensing reconstruction based on structured regularization*. to be submitted.

Carole Lazarus, Pierre Weiss, Nicolas Chauffert, Franck Mauconduit, Loubna El Gueddari, Christophe Destrieux, Ilyess Zemmoura, Alexandre Vignaud and Philippe Ciuciu. *SPARKLING: variable density k-space filling curves for accelerated* T_2^**-weighted MRI*. Journal of Magnetic Resonance in Medicine, vol. 81, no. 6, pp. 3643-3661, 2019.

Carole Lazarus, Pierre Weiss, Loubna El Gueddari, Franck Mauconduit, Alexandre Vignaud and Philippe Ciuciu. *3D SPARKLING trajectories for high-resolution* T_2^**-weighted Magnetic Resonance imaging*. NMR in Biomedicine. In revision.

Antoine Grigis, Samuel Farrens, Loubna El Gueddari, Jean-Luc Starck, Philippe Ciuciu. *PySAP: Python Sparse Data Analysis Package for Multidisciplinary Image Processing*. Submitted

Publications II

International Conferences Paper Presented with Reading Committee and Proceedings

Loubna El Gueddari, Emilie Chouzenoux, Alexandre Vignaud, Jean-Christophe Pesquet, Philippe Ciuciu. *Online MR image reconstruction for compressed sensing acquisition in T2* imaging*. Proceedings of the Wavelets: Applications in Signal and Image Processing XVIII, San Diego, CA, USA, 2019. Oral.

Loubna El Gueddari, Philippe Ciuciu, Emilie Chouzenoux, Alexandre Vignaud, Jean-Christophe Pesquet. *Calibrationless OSCAR-based image reconstruction in compressed sensing parallel MRI*. Proceedings of the IEEE International Symposium of Biomedical Imaging, Venice, Italy, 2019. Oral.

Loubna El Gueddari, Emilie Chouzenoux, Alexandre Vignaud, Jean-Christophe Pesquet, Philippe Ciuciu. *Online MR image reconstruction for compressed sensing acquisition in T2* imaging*. Proceedings of the Wavelets: Applications in Signal and Image Processing XVIII, San Diego, CA, USA, 2019. Oral.

Loubna El Gueddari, Carole Lazarus, Hanaé Carrié, Alexandre Vignaud, Philippe Ciuciu. *Self-calibrating nonlinear reconstruction algorithms for variable density sampling and parallel reception MRI*. Proceedings of the 10th IEEE Sensor Array and Multichannel Signal Processing Workshop (SAM), Shefield, UK, 2018. Oral.

Hamza Cherkaoui, Loubna El Gueddari, Carole Lazarus, Antoine Grigis, Fabrice Poupon, Alexandre Vignaud, Samuel Farrens, Jean-Luc Starck, Philippe Ciuciu. *Analysis Vs Synthesis-based Regularization for Combined Compressed Sensing and Parallel MRI Reconstruction at 7 Tesla*. Proceedings of the 26th Europeean Signal Processing Conference, Rome, Italy, 2018

Publications III

Abstracts Presented at International Conferences with Reading Committee and Proceedings

Loubna El Gueddari, Emilie Chouzenoux, Jean-Christophe Pesquet, Alexandre Vignaud and Philippe Ciuciu. *OSCAR-based reconstruction for compressed sensing and parallel MR imaging*. Proceedings of the 27th Annual Meeting of the International Society for Magnetic Resonance in Medicine, Montreal, Canada, 2019. ePoster.

Loubna El Gueddari, Emilie Chouzenoux, Jean-Christophe Pesquet, Alexandre Vignaud and Philippe Ciuciu. *Online compressed sensing MR image reconstruction for high resolution* $T2^*$ *imaging*. Proceedings of the 27th Annual Meeting of the International Society for Magnetic Resonance in Medicine, Montreal, Canada, 2019. ePoster.

Carole Lazarus, Pierre Weiss, Nicolas Chauffert, Franck Mauconduit, Loubna El Gueddari, Christophe Destrieux, Ilyess Zemmoura, Alexandre Vignaud and Philippe Ciuciu. *SPARKLING: variable-density k-space filling curves for accelerated MRI*. Proceedings of the 27th Annual Meeting of the International Society for Magnetic Resonance in Medicine, Montreal, Canada, 2019. ePoster.

Loubna El Gueddari, Carole Lazarus, Hanaé Carrié, Alexandre Vignaud and Philippe Ciuciu. *Self-calibrating nonlinear MR image reconstruction algorithms for variable density sampling and parallel imaging*. Proceedings of the 28th Annual Meeting of the International Society for Magnetic Resonance in Medicine, Paris, France, 2018. ePoster.

Publications IV

Abstracts Presented at International Conferences with Reading Committee and Proceedings

Carole Lazarus, Pierre Weiss, Loubna El Gueddari, Franck Mauconduit, Alexandre Vignaud and Philippe Ciuciu. *Distribution-controlled and optimally spread non-Cartesian sampling curves for accelerated in vivo brain imaging at si 7T*. Proceedings of the 28th Annual Meeting of the International Society for Magnetic Resonance in Medicine, Paris, France, 2018. ePoster.

Loubna El Gueddari, Carole Lazarus, Hamza Cherkaoui, Elvis Dohmatob, Alexandre Vignaud, Philippe Ciuciu. *Self-calibrating non-linear reconstruction algorithm for variable density sampling and parallel reception MRI*. Proceedings of the IEEE International Symposium of Biomedical Imaging, Washington D.C., USA, 2018. Poster

Hanaé Carrié, Loubna El Gueddari, Hamza Cherkaoui, Elvis Dohmatob, Lisa Leroi, Philippe Ciuciu. *Multi-Contrast Dictionary Learning for 2D Compressed Sensing MRI Reconstruction*. Proceedings of the IEEE International Symposium of Biomedical Imaging, Washington D.C., USA, 2018.

Martin Jacob, Loubna El Gueddari, Gabriele Navarro, Cyrille Marie-Claire, Pascale Bayle-Guillemaud, Philippe Ciuciu, Zineb Saghi. *Statistical Machine Learning and Compressed Sensing Approaches for Analytical Electron Tomography - Application to Phase Change Materials*. Proceedings of Microscopy and Microanalysis, Portland, Oregon, 2019.

Thank you for your attention

References I

Argyriou, Andreas, Rina Foygel, and Nathan Srebro (2012). “Sparse Prediction with the k-Support Norm”. In: *NeurIPS*, pp. 1457–1465.

Bondell, H.D. and B.J. Reich (2008). “Simultaneous regression shrinkage, variable selection, and supervised clustering of predictors with OSCAR”. In: *Biometrics* 64.1, pp. 115–123.

Candès, Emmanuel J., J. Romberg, and T. Tao (2006). “Robust uncertainty principles: exact signal reconstruction from highly incomplete frequency information”. In: *IEEE Transactions on information theory* 52.2, pp. 489–509.

Chun, I.Y., B. Adcock, and T.M. Talavage (2016). “Efficient compressed sensing SENSE pMRI reconstruction with joint sparsity promotion”. In: *IEEE Transactions on Medical Imaging* 35.1, pp. 354–368.

Condat, Laurent (2013). “A primal–dual splitting method for convex optimization involving Lipschitzian, proximable and linear composite terms”. In: *Journal of Optimization Theory and Applications* 158.2, pp. 460–479.

References II

- El Gueddari, Loubna et al. (2018). "Self-Calibrating Nonlinear Reconstruction Algorithms for Variable Density Sampling and Parallel Reception MRI". In: *IEEE SAM workshop.*
- El Gueddari, Loubna et al. (2019a). "Calibrationless OSCAR-based image reconstruction in compressed sensing parallel MRI". In: *ISBI 2019.*
- – (2019b). "Online compressed sensing MR image reconstruction for high resolution T2* imaging". In: *Proceedings of the 27th Annual Meeting of ISMRM*, p. 4679.
- El Gueddari, Loubna et al. (2019c). "Online MR image reconstruction for compressed sensing acquisition in T2* imaging.". In: *Wavelets: Applications in Signal and Image Processing XVIII.*
- El Gueddari, Loubna et al. (2020). "PySAP-MRI: a Python Package for MR Image Reconstruction". In: *ISMRM workshop on Data Sampling.*
- Haldar, Justin P and Jingwei Zhuo (2016). "P-LORAKS: Low-rank modeling of local k-space neighborhoods with parallel imaging data". In: *Magnetic resonance in medicine* 75.4, pp. 1499–1514.
- Hansen, Michael Schacht and Thomas Sangild Sørensen (2013). "Gadgetron: an open source framework for medical image reconstruction". In: *Magnetic resonance in medicine* 69.6, pp. 1768–1776.

References III

Krupa, Katarzyna and Monika Bekiesińska-Figatowska (2015). “Artifacts in magnetic resonance imaging”. In: *Polish journal of radiology* 80, p. 93.

Lazarus, Carole et al. (2019). “SPARKLING: variable-density k-space filling curves for accelerated T2*-weighted MRI”. In: *Magnetic Resonance in Medicine* 81.6, pp. 3643–3661.

Lin, Jyh-Miin (2018). “Python Non-Uniform Fast Fourier Transform (PyNUFFT): An Accelerated Non-Cartesian MRI Package on a Heterogeneous Platform (CPU/GPU)”. In: *Journal of Imaging* 4.3, p. 51.

Lustig, Miki, D. Donoho, and John M. Pauly (2007). “Sparse MRI: The application of compressed sensing for rapid MR imaging”. In: *Magnetic Resonance in Medicine* 58.6, pp. 1182–1195.

Majumdar, Angshul and Rabab Ward (2012). “Calibration-less multi-coil MR image reconstruction”. In: *Magnetic Resonance in Medicine* 30.7, pp. 1032–1045.

Moreau, Jean Jacques (1962). “Fonctions convexes duales et points proximaux dans un espace hilbertien”. In: *Comptes Rendus de l'Académie des Sciences de Paris.*

References IV

- Pohmann, Rolf, Oliver Speck, and Klaus Scheffler (2016). "Signal-to-noise ratio and MR tissue parameters in human brain imaging at 3, 7, and 9.4 tesla using current receive coil arrays". In: *Magnetic resonance in medicine* 75.2, pp. 801–809.
- Roemer, P.B. et al. (1990). "The NMR phased array". In: *Magnetic Resonance in Medicine* 16.2, pp. 192–225.
- Samsonov, Alexei A et al. (2004). "POCSENSE: POCS-based reconstruction for sensitivity encoded magnetic resonance imaging". In: *Magnetic Resonance in Medicine* 52.6, pp. 1397–1406.
- Stucht, Daniel et al. (2015). "Highest resolution in vivo human brain MRI using prospective motion correction". In: *PloS one* 10.7, e0133921.
- Uecker, M. et al. (2014). "ESPIRiT– an eigenvalue approach to autocalibrating parallel MRI: where SENSE meets GRAPPA". In: *Magnetic Resonance in Medicine* 71.3, pp. 990–1001.
- Vũ, B.C (2013). "A splitting algorithm for dual monotone inclusions involving cocoercive operators". In: *Advances in computational mathematics* 38.3, pp. 667–681.

References V

Yuan, Ming and Yi Lin (2006). "Model selection and estimation in regression with grouped variables". In: *Journal of the Royal Statistical Society: Series B (Statistical Methodology)* 68.1, pp. 49–67.

Zwanenburg, Jaco JM et al. (2010). "Fluid attenuated inversion recovery (FLAIR) MRI at 7.0 Tesla: comparison with 1.5 and 3.0 Tesla". In: *European radiology* 20.4, pp. 915–922.